Chinese Journal of
POLYMER SCIENCE

RAPID COMMUNICATION

https://doi.org/10.1007/s10118-026-3809-0
Chinese J. Polym. Sci.

High Pressure Synthesis for Gold-backboned Polymer

Fuyao Huang[a,†], Xingyu Chen[b,†], Zihao Zhao[a,†], Yifeng Zhang[a], Yuhong Mao[b], Kainan Hong[a], Hao Guo[a], Haiyang Cheng[a], Meng Liao[a], Xujie Lü[b*], and Huisheng Peng[a*]

[a] *State Key Laboratory of Molecular Engineering of Polymers, Department of Macromolecular Science, and Institute of Fiber Materials and Devices, Fudan University, Shanghai 200438, China*
[b] *Center for High Pressure Science and Technology Advanced Research, Shanghai 201203, China*

Electronic Supplementary Information

Abstract Metal-backboned polymers, featuring one-dimensional atomic chains held together by metal–metal bonds, represent a highly promising class of functional materials. However, current synthetic methods rely on solution-phase multidentate bridging ligands, which severely limit the degree of polymerization. Herein, we report a pressure-driven solid-phase polymerization strategy that directly forms intermolecular Au—Au bonds from a dinuclear gold precursor at a pressure of 25 GPa, yielding a gold-backboned polymer (GBP). This method produces a continuous one-dimensional gold chain comprising more than 100 gold atoms. The peripheral ligands coordinate around the backbone, stabilizing the chain and endowing the polymer with high solution processability. The resulting GBP exhibited high thermal stability, well-defined glass transition temperature, and broad-spectrum photoluminescence spanning from the visible to near-infrared regions. This study opens a new synthetic route to long-chain metal-backboned polymers and provides a structurally well-defined model system for investigating the intrinsic photophysical properties of one-dimensional metal–metal bonds.

Keywords Metal-backboned polymer; Metal–metal bond; High pressure; Polymerization; Electron delocalization

Citation: Huang, F.; Chen, X.; Zhao, Z.; Zhang, Y.; Mao, Y.; Hong, K.; Guo, H.; Cheng, H.; Liao, M.; Lü, X.; Peng, H. High pressure synthesis for gold-backboned polymer. *Chinese J. Polym. Sci*. https://doi.org/10.1007/s10118-026-3809-0

INTRODUCTION

Metal-backboned polymers (MBPs) represent an emerging class of materials in which the polymer backbone consists solely of metal atoms connected by metal–metal bonds.[1,2] This one-dimensional metallic chain structure is expected to promote electron delocalization and quantum confinement along the backbone, leading to optical and electronic properties superior to those of conventional polymers.[3–7] However, current synthesis routes to MBPs rely on multidentate bridging ligands to stabilize inherently weak metal-metal interactions. This requirement severely limits the degree of polymerization and leaves the ligands anchored to the backbone, thereby shielding the intrinsic electronic structure of the metal backbone.[3,8,9]

Gold is a promising candidate for constructing MBPs because its Au—Au interactions exhibit both a suitable bond strength and a broad effective range.[10] Au—Au chains can be found in crystalline solids,[11] but it remains unavailable to achieve continuous Au—Au bonding to form MBPs. High-pressure chemistry offers powerful thermodynamic leverage to dramatically compress intermolecular distances, manipulate orbital overlaps, and drive reactions along pathways inaccessible *via* traditional means.[12–14] In particular, compressing a preorganized crystalline monomer in the solid state can restrict molecular motion and facilitate topochemical-like polymerization, directly forming Au—Au bonds without the need for solvent assistance or structural templates. Consequently, this method offers a viable approach for solid-phase construction of MBPs.

In this study, for the first time, we discovered a high-pressure solid-phase polymerization strategy that converts a dinuclear gold complex precursor into a gold-backboned polymer (GBP) through the direct formation of Au—Au bonds under a pressure of 25 GPa (Fig. 1). Peripheral bis(diphenylphosphino)methane (DPPM) ligands interlock around the gold chain, stabilizing the one-dimensional GBP while endowing the polymer with solution processability. *In situ* high-pressure synchrotron X-ray diffraction and Raman spectroscopy revealed preferential compression of the crystallographic *b*-axis, stepwise formation of intermolecular Au—Au bonds, and eventual homogenization of bond lengths. The resulting GBP possessed an average chain length exceeding 100 gold atoms and exhibited high thermal stability and broadband photoluminescence in the visible to near-infrared regions.

* Corresponding authors, E-mail: xujie.lu@hpstar.ac.cn (X.L.)
E-mail: penghs@fudan.edu.cn (H.P.)
† These authors contributed equally to this work.
Received June 27, 2026; Accepted July 8, 2026; Published online August 5, 2026

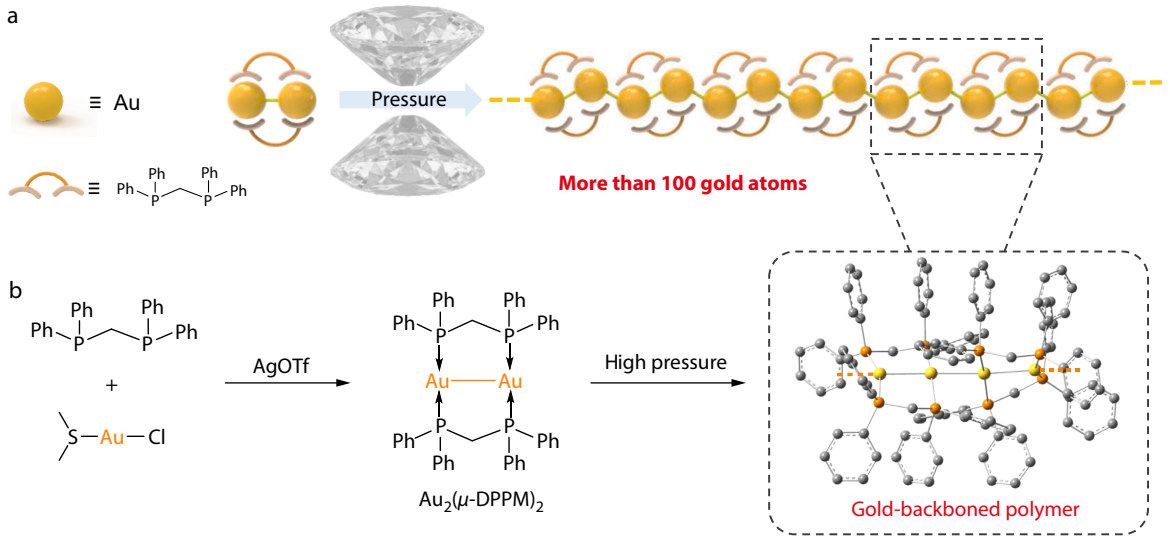

Fig. 1 Structure and synthetic approach to GBP. (a) Schematic architecture of the molecular structure; (b) Synthetic approach.

EXPERIMENTAL

The details of experiments are included in the electronic supplementary information (ESI).

RESULTS AND DISCUSSION

Synthesis and Structural Characterization of the Monomer and GBP

The dinuclear gold precursor $Au_2(\mu\text{-DPPM})_2(OTf)_2$ was synthesized (Figs. S1–S3 in ESI).[15] Single-crystal X-ray diffraction (Fig. 2a, Table S1 in ESI) revealed that the two gold atoms were bridged by DPPM ligands, with intramolecular Au—Au distances of 2.93–2.96 Å. The gold atoms were oriented along the crystallographic *b*-axis, and the phenyl rings of DPPM were interdigitated, providing a preorganized pathway for the formation of intermolecular Au—Au bonds under high pressure. Raman spectroscopy conforms to density functional theory calculations (Fig. 2b), showing a strong Au—Au stretching vibration at 76 cm^{-1}. The minor discrepancies arise mainly from solid-state lattice effects. The UV-Vis absorption spectra (Figs. S4a and S4b in ESI) exhibited a distinct Au—Au metal-metal charge-transfer band in the visible region.[16] These results collectively confirm the preorganized orientation of the Au atoms and the presence of intramolecular Au—Au interactions in the monomer.

The monomer was placed in a diamond anvil cell and slowly compressed to 25 GPa, which shortened the intermolecular distances along the *b*-axis and induced the formation of intermolecular Au—Au bonds. The GBP was obtained after decompression to ambient pressure. Gel permeation chromatography coupled with multi-angle static light scattering showed a weight-average molecular weight (M_w) of 63.7 kDa and a dispersity ($Đ$) of 1.249 (Fig. 2c), corresponding to about 108 gold atoms per chain, with a measured d*n*/d*c* value of 0.1225 mL/g (Fig. S5 in ESI). Here $Đ$ represents dispersity of soluble fraction, as a very small amount of insoluble material, possibly higher-molecular-weight species, was observed upon dissolution of the recovered product. The XPS C 1s spectra (Fig. 2f) show that the sp^2-C/sp^3-C ratio remained essentially unchanged from the monomer to the polymer, indicating that the DPPM ligands did not undergo decomposition or chemical reactions during the high-pressure process and remained coordinated through Au—P bonds. This conclusion was further supported by ^1H and ^{31}P nuclear magnetic resonance spectra (Figs. S6 and S7 in ESI). High-resolution transmission electron microscopy (Fig. 2d and Figs. S8a–S8c in ESI) revealed an amorphous morphology, and energy-dispersive X-ray spectroscopy mapping (Figs. S8d–S8f in ESI) show a uniform distribution of Au and P. Scanning transmission electron microscopy (Fig. 2e) directly revealed a local segment of the polymer chain, where gold atoms were continuously arranged with mild bending and no branches or crosslinks. Although this local image represents only a fragment of the overall chain, it provides direct evidence of a linear one-dimensional structure held together by Au—Au bonds.

Au L_3-edge X-ray absorption spectroscopy (Figs. 2g–2i and Fig. S9 in ESI) further elucidates the local coordination environment of the gold chain. The X-ray absorption near-edge structure spectra (Fig. 2g) showed a white line intensity characteristic of Au(I), consistent with the X-ray photoelectron spectroscopy Au 4f results (Fig. S10 in ESI), confirming that the oxidation state of Au remained unchanged during the high-pressure process. The Fourier-transformed extended X-ray absorption fine structure spectra (Fig. 2h) exhibited two peaks at about 1.76 and 2.91 Å. Wavelet transform analysis (Fig. 2i) assigned the low-*k* peak (5–8 $Å^{-1}$) to Au—P scattering from the peripheral DPPM ligands and the high-*k* peak (7–9 $Å^{-1}$) to Au—Au scattering.[17] Least-squares fitting gave Au—Au coordination numbers of 2.2±0.3, slightly above 2 because of possible end-chain effects or fitting uncertainty, but was fully consistent with a linear one-dimensional chain model. Together, these results support the formation of a continuous one-dimensional Au—Au-bonded metal backbone in GBP, with peripheral DPPM ligands stabilizing the structure through Au—P coordination.

Structural Evolution and Mechanism of the High-pressure Polymerization Process

To elucidate the microstructural evolution mechanism of the

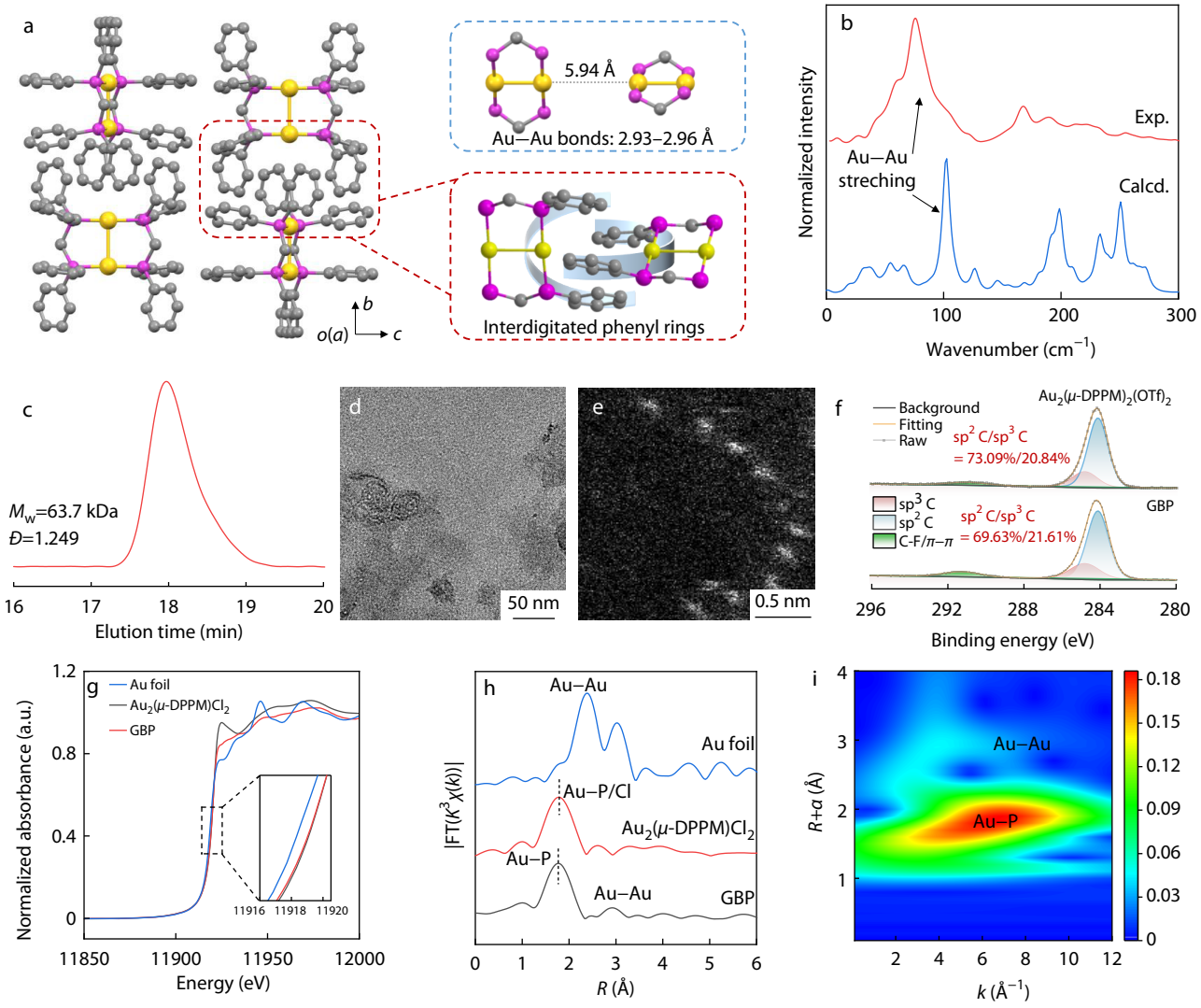

Fig. 2 Characterization of the monomer $Au_2(\mu\text{-DPPM})_2(OTf)_2$ and the GBP. (a) Single-crystal X-ray structure of the monomer. Here, solvent molecules and counterions are omitted for clarity; (b) Experimental and density functional theory-calculated Raman spectra of the monomer; (c) Gel permeation chromatography multi-angle static light scattering trace of GBP; (d) High-resolution transmission electron microscopy image; (e) Scanning transmission electron microscopy image; (f) X-ray photoelectron spectroscopy C 1s spectra of the monomer and GBP; (g) Au L_3-edge X-ray absorption near-edge structure spectra of GBP and reference compounds; (h) Fourier-transformed extended X-ray absorption fine structure spectra of GBP; (i) Wavelet transform analysis of the extended X-ray absorption fine structure signal.

pressure-driven polymerization of the monomer into GBP through intermolecular Au—Au bond formation, we performed *in situ* high-pressure synchrotron powder X-ray diffraction measurements using a diamond anvil cell. The diffraction patterns at various pressures are shown in Fig. 3(a), Figs. S11 and S12 (in ESI). Based on the ambient-pressure crystal structure, 2θ diffraction peaks of the {400} family of planes for the *a*, *b*, and *c* axes were identified at 4.996°, 6.047°, and 4.978°, respectively. These peaks shifted to higher angles with increasing pressure, indicating a reduction in interplanar spacing. The corresponding *d*-spacing as a function of the pressure is plotted in Fig. 3(b).

The compression of the unit cell was anisotropic. By comparing the compression rates along the *b*-axis and *a*-axis, we obtained the relative compression ratio curve (right axis of Fig. 3b). In the 0–5.20 GPa region, the *b*-axis compressed significantly faster than the *a*-axis, demonstrating preferential compression. Because the *b*-axis direction coincides with the direction of intermolecular Au—Au interactions, the preferential contraction of the *b*-axis at low pressure indicates that intermolecular Au—Au interactions are preferentially enhanced and trigger bond formation, providing structural evidence for pressure-induced formation of GBP (Note S1 in ESI). As pressure increases over 5.20 GPa, the compression rate of the *b*-axis relative to the *a*-axis was slowed down, indicating that after intermolecular Au—Au bond formation, the system enters a stage of densification and homogeneous compression.

The evolution of *in situ* high-pressure Raman spectroscopy further corroborated the structural changes. As shown in Fig. 3(c), Figs. S13 and S14 (in ESI), the Raman peak at 76 cm^{-1} under ambient pressure corresponds to the characteristic Au—Au stretching mode.[18] With increasing pressure, this peak shifts to higher wavenumbers, indicating phonon hard-

https://doi.org/10.1007/s10118-026-3809-0

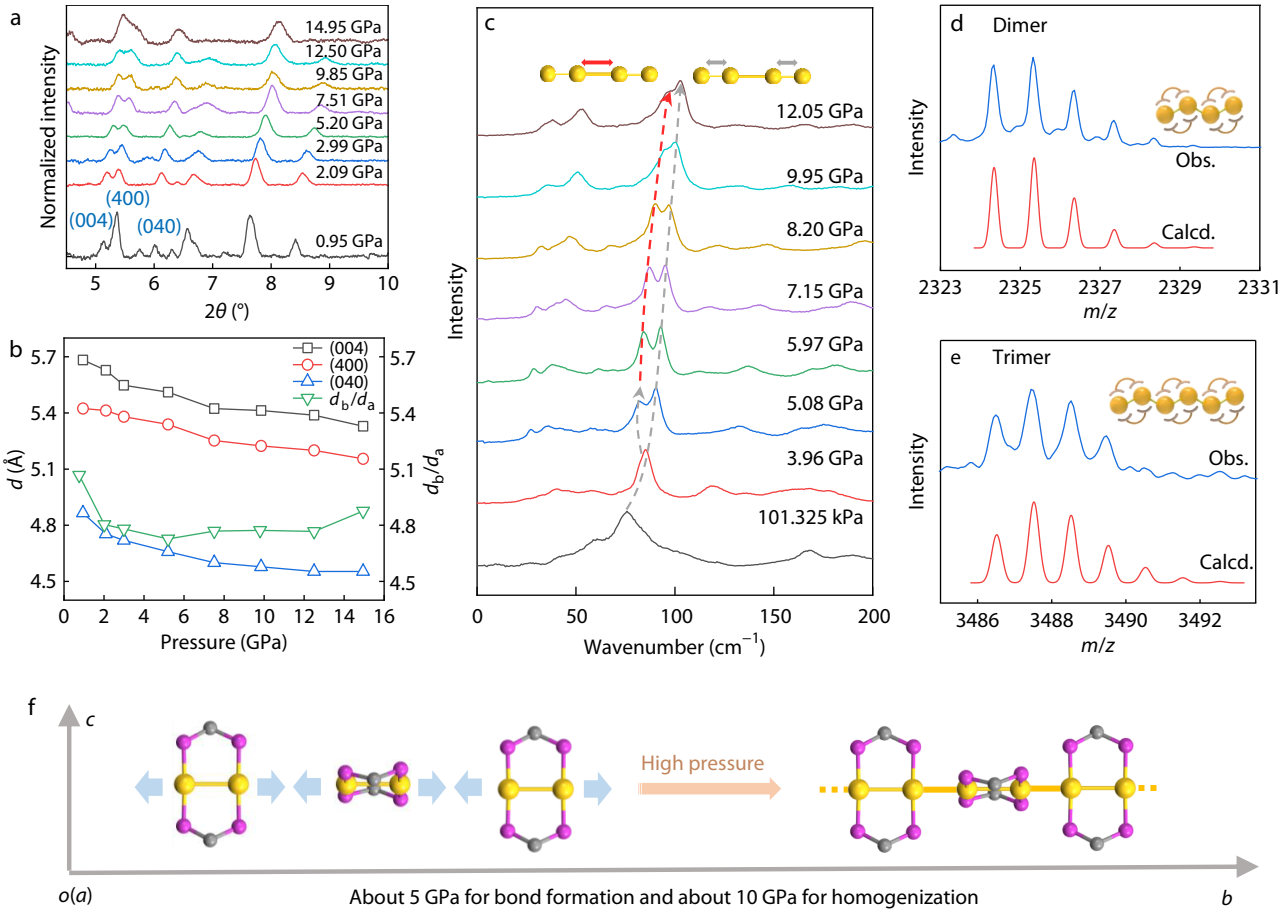

Fig. 3 *In situ* high-pressure structural evolution and polymerization mechanism. (a) *In situ* synchrotron X-ray diffraction patterns of the monomer and GBP at selected pressures; (b) Pressure dependence of the *d*-spacings for the {400} family of planes along the *a*, *b*, and *c* axes (left) and the compression rate of the *b*-axis relative to the *a*-axis (right), showing preferential compression of the *b*-axis; (c) *In situ* high-pressure Raman spectra; (d, e) Magnified matrix assisted laser desorption/ionization time-of-flight mass analysis of the dimer and trimer obtained under lower pressure, respectively; (f) Schematic illustration of the pressure-induced polymerization pathway. Color code: gray = carbon, purple = phosphorus, yellow = gold.

ening. At 5.08 GPa, the original single peak splits into a weaker low-frequency peak and a stronger high-frequency peak. Combined with the X-ray diffraction results, the intermolecular Au—Au distance along the *b*-axis was shortened significantly at this pressure, and the relative compression ratio d_b/d_a reached its minimum, bringing the intermolecular Au—Au interactions to a critical state. Therefore, the newly emerging low-frequency peak was assigned to intermolecular Au—Au vibrations, whereas the high-frequency peak was assigned to intramolecular Au—Au vibrations. With further increase in pressure, the intensity of the intermolecular Au—Au peak continuously increased and eventually became comparable to that of the intramolecular peak, forming a doublet of similar intensities. This indicates that the intramolecular and intermolecular Au—Au bond lengths are similar. At a pressures of 9.95 GPa, the two peaks gradually merged, and the peak position and shape became uniform, demonstrating the homogenization of Au—Au bond lengths and bond strengths throughout the system. At this stage, no significant difference remained between the intra- and intermolecular Au—Au interactions, and a continuous, uniform, one-dimensional Au atomic chain was formed.

Furthermore, magnified matrix-assisted laser desorption/ionization time-of-flight mass analysis of the product obtained under lower pressure detected signals corresponding to dimers and trimers (Figs. 3d and 3e). Density functional theory calculations were performed on the dimer and trimer to understand the local bonding within the polymer backbone (Figs. S15 and S16 in ESI). The optimized structures showed that in the dimer, four gold atoms were sequentially connected and wrapped by DPPM ligands, with Au—Au distances of 2.689, 2.721, and 2.755 Å, indicating strong Au—Au interactions. The peripheral ligands in this interlocking structure protect the inner gold atomic chain and prevent solvation, thereby laying the foundation for the solution processability of GBP. The trimers exhibited similar features. Further analyses of the Mayer bond order, interaction region indicator, and electron localization function values also supported the existence of continuous Au—Au bonds (Figs. S17–S20, Note S2 in ESI). These results demonstrate that, as the chain grows, similar Au—Au interactions exist in the oligomers, providing a basis for the formation of GBP. Based on the above results, Fig. 3(f) schematically illustrates the high-pressure polymerization pathway, where pressure first compress-

https://doi.org/10.1007/s10118-026-3809-0

es the *b*-axis, promotes the formation of intermolecular Au—Au bonds at about 5.0 GPa, and homogenizes the bond lengths at about 10 GPa, ultimately yielding a GBP consisting of continuous Au—Au bonds.

Intrinsic Properties of GBP at Ambient Pressure

Next, we investigated the intrinsic properties of GBP. Thermogravimetric analysis showed an onset decomposition temperature (T_d) of approximately 306 °C, with a residual mass of 40.3% at 800 °C (Fig. 4a, Note S3 in ESI), indicating that high thermal stability is sufficient for conventional processing. Differential scanning calorimetry revealed a well-defined glass transition temperature (T_g) of 54.8 °C (Fig. 4b), demonstrating that GBP is in a glassy state at room temperature. Annealing near T_g is expected to induce chain rearrangement and potentially affect the intrinsic properties of GBP. In contrast to the dinuclear gold precursor, which lacks segmental cooperative motion, this result directly confirms the polymer nature of GBP that the continuous Au—Au bonds link gold atoms into long chains capable of segmental relaxation.

Owing to the heavy-atom effect of gold, gold complexes typically exhibit bright phosphorescence in the solid state.[19,20] We investigated the intrinsic photoluminescence properties of GBP under ambient conditions. The excitation spectra revealed two optimal excitation wavelengths, 380 and 430 nm (Fig. S21 in ESI). The emission spectra of GBP demonstrated a wide emission band covering the visible to near-infrared region from 400 to 850 nm (Fig. 4c). Notably, under 380 nm excitation, the prompt and delayed emission spectra exhibited nearly identical profiles (Fig. S22 in ESI), indicating that the emission of GBP is long-lived and can be assigned to triplet-state phosphorescence. In contrast to discrete dinuclear gold complexes, the continuous Au—Au bonds in GBP not only extend the emission wavelength into the near-infrared region, but also modulate the phosphorescence behavior through metal-metal charge transfer transitions. Meanwhile, GBP exhibits a narrow-bandgap semiconducting nature, with an electronic bandgap of 2.03 eV (Fig. S23 in ESI), consistent with the delocalized electronic structure along the Au—Au backbone. This finding demonstrates that the continuous Au—Au interactions along the one-dimensional gold backbone are the key structural origin of the broad spectrum, near-infrared phosphorescence in GBP.

Optical Monitoring of the High-pressure Polymerization Process and Optical Properties of the GBP under High Pressure

To track the optical response of the monomer during its pressure-driven polymerization into GBP *via* Au—Au bond formation, we performed *in situ* high-pressure UV-Vis absorption and

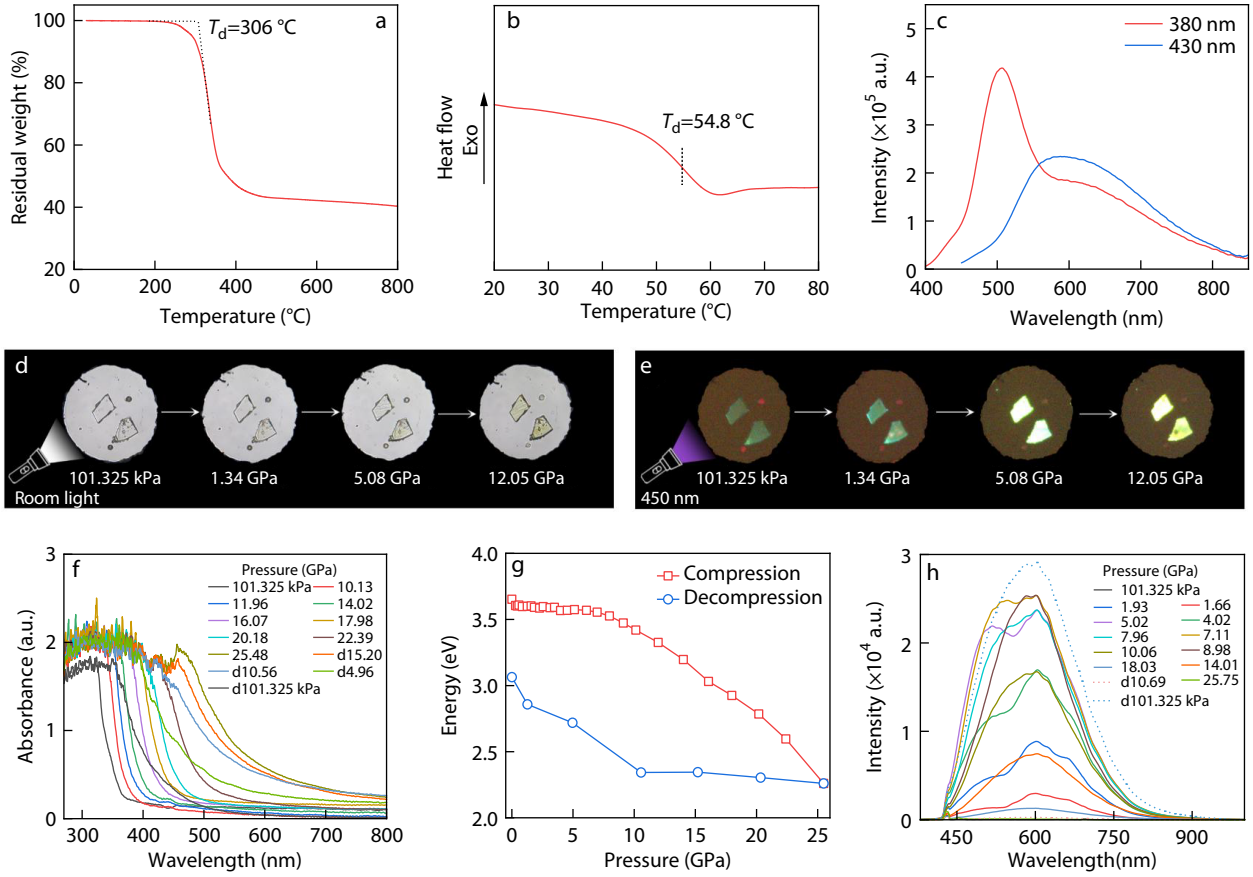

Fig. 4 Intrinsic properties of GBP at ambient pressure and optical responses under high pressure. (a) Thermogravimetric analysis and (b) differential scanning calorimetry curves of GBP, respectively; (c) Photoluminescence emission spectra of GBP under excitation at 380 and 430 nm; (d, e) Optical and luminescent photographs of the sample under different pressures, respectively; (f) *In situ* UV-Vis absorption spectra and (g) bandgap evolution of the monomer and GBP during compression and decompression, respectively; (h) *In situ* high-pressure photoluminescence emission spectra (excitation wavelength of 405 nm).

https://doi.org/10.1007/s10118-026-3809-0

photoluminescence spectroscopy. As shown in the UV-Vis absorption spectra (Figs. 4f and 4g), the optical absorption edge of the monomer was continuously red-shifted with increasing pressure, accompanied by a progressive darkening of the crystal color (Fig. 4d). When the pressure exceeded 20 GPa, an irreversible structural transformation occurred. During decompression, the absorption edge did not recover along the compression path but remained redshifted. This irreversibility indicates that high pressure induces a new electronic structure that is stable under ambient conditions, which is consistent with the formation of continuous Au—Au bonds in GBP.

In situ high-pressure photoluminescence spectra (Figs. 4e and 4h) showed that the emission signal of the monomer under ambient pressure was very weak at an excitation wavelength of 405 nm. As the pressure increased, the emission intensity first increased sharply and then decreased gradually (Fig. S24 in ESI). In the range from 101.325 kPa to 7.11 GPa (Fig. 4h and Fig. S25 in ESI), the intensity continuously increased, reaching a maximum of 1362 times the initial value. Upon further compression to 20 GPa (Fig. 4h and Fig. S26 in ESI), when the sample underwent amorphization, the emission decayed to a level comparable to the initial one. During decompression, the emission intensity steadily recovered and, upon full release to ambient pressure, reached the highest value of the entire experiment, 1604 times the initial intensity (Fig. 4h and Fig. S27 in ESI). This enhancement reflects the retention of Au—Au bonds formed under high pressure and the partial annealing of non-radiative decay upon decompression. Notably, the shape of the emission peak also evolved significantly during compression. In the low-pressure regime, the spectrum exhibited multiple peaks that gradually merged with increasing pressure and eventually formed a single broadened peak. This evolution indicates that pressure continuously modulates intra-and intermolecular interactions, enhancing Au—Au interactions and causing the originally discrete excited-state energy levels to converge and homogenize. The single-peak feature was retained after decompression, demonstrating that the high-pressure-induced long-chain Au—Au polymer structure remained stable.

Combined with the structural characterization results (Figs. 3a–3c and Figs. S11–S13 in ESI), the organic ligands underwent irreversible amorphization above 20 GPa, and the long-range crystalline order was destroyed, leading to the disappearance of the diffraction and Raman signals. This further confirms that the emission center of the system is not an organic ligand, but rather a metal-based luminescent site dominated by Au—Au interactions. The multiple peaks at low pressures correspond to isolated dinuclear gold units with different local environments in the crystalline state. Under pressure, adjacent units gradually bond to form a continuous polymer chain, and the luminescent sites become uniform, ultimately resulting in a single-peak emission. These Au—Au polymeric luminescent sites remained stable for a long period after decompression, providing direct structure–property correlation evidence for the photoluminescence of GBP.

CONCLUSIONS

In summary, we developed a high-pressure solid-phase synthesis strategy to successfully convert a dinuclear gold complex precursor into GBP, with each chain containing an average of about 108 linearly arranged gold atoms. *In situ* high-pressure synchrotron X-ray diffraction and Raman spectroscopy revealed that pressure preferentially compresses the crystallographic *b*-axis, drives the formation of intermolecular Au—Au bonds, and ultimately yields a continuous and uniform one-dimensional Au chain. The resulting GBP is soluble in common organic solvents and exhibits high thermal stability and a well-defined glass transition temperature, confirming its polymeric nature. Photoluminescence studies show that GBP displays broad-spectrum emission spanning the visible to near-infrared region, and the high agreement between the prompt and delayed emission spectra indicates its phosphorescent character. Their unique structure and optical properties endow GBPs with promising applications in optoelectronics, energy harvesting, and catalysis. This study establishes high-pressure solid-phase polymerization as a general synthesis method for long-chain, solution-processable MBPs, providing a precise model system for investigating one-dimensional metal-metal interactions and their intrinsic photophysical properties.

Conflict of Interests

Huisheng Peng is an editorial board member for *Chinese Journal of Polymer Science* and was not involved in the editorial review or the decision to publish this article. The authors declare no interest conflict.

Electronic Supplementary Information

Electronic supplementary information (ESI) is available free of charge in the online version of this article at http://doi.org/10.1007/s10118-026-3809-0.

Data Availability Statement

The data supporting the findings of this study are available from the corresponding authors upon reasonable request.

ACKNOWLEDGMENTS

This work was financially supported by the Ministry of Science and Technology of the People's Republic of China (Nos. 2022YFA1203001 and 2022YFA1203002) and the National Natural Science Foundation of China (Nos. T2321003, T2596011, T2596012, 22335003, and 22275004). The authors would like to thank Dr. Zhengwang Liu from Fudan University for his assistance with the high-resolution transmission electron microscopy. The authors also acknowledge Dr. Kaiwen Zeng for his assistance with data analysis and discussion.

REFERENCES

1 Zeng, K.; Peng, H. Metal-backboned polymer: conception, design and synthesis. *Chinese J. Polym. Sci.* **2023**, *41*, 3–6.
2 Zhang, Y.; Zeng, K.; Peng, H. Metal-backboned polymer: concept,

Graphical Abstract

High Pressure Synthesis for Gold-backboned Polymer

Fuyao Huang, Xingyu Chen, Zihao Zhao, Yifeng Zhang, Yuhong Mao, Kainan Hong, Hao Guo, Haiyang Cheng, Meng Liao, Xujie Lü, and Huisheng Peng

Fudan University; Center for High Pressure Science and Technology Advanced Research

High-pressure solid-phase polymerization directly converts a dinuclear gold complex into a gold-backboned polymer with each chain containing over 100 gold atoms, whose one-dimensional Au backbone enables efficient electron delocalization and broad phosphorescence.

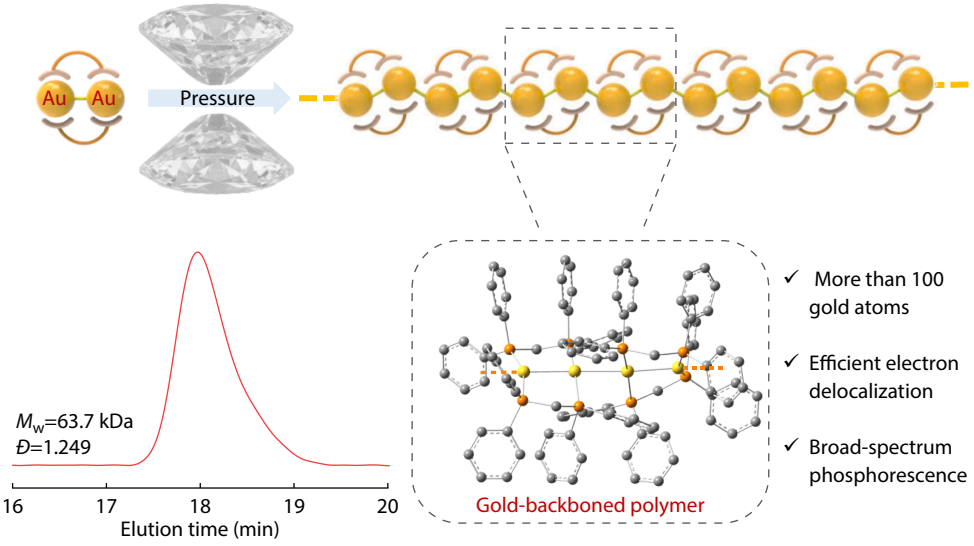

Chinese J. Polym. Sci., 2026 *https://doi.org/10.1007/s10118-026-3809-0*

advance and perspective. *Sci. China Mater.* **2025**, *68*, 105−109.
3 Zeng, K.; Yang, Y.; Xu, J.; Wang, N.; Tang, W.; Xu, J.; Zhang, Y.; Wu, Y.; Xu, Y.; Wang, G.; Chen, P.; Wang, B.; Sun, X.; Jin, G.; Peng, H. Metal-backboned polymers with well-defined lengths. *Angew. Chem. Int. Ed.* **2023**, *62*, e202216060.
4 Greenfield, J. L.; DiNuzzo, D.; Evans, E. W.; Senanayak, S. P.; Schott, S.; Deacon, J. T.; Peugeot, A.; Myers, W. K.; Sirringhaus, H.; Friend, R. H.; Nitschke, J. R. Electrically induced mixed valence increases the conductivity of copper helical metallopolymers. *Adv. Mater.* **2021**, *33*, 2100403.
5 Moriyama, H.; Otsubo, K.; Sugimoto, K.; Kawaguchi, S.; Kitagawa, H. Observation of an alternate charge-polarization state in a one-dimensional Pt−Pt−I chain compound with a bulky pendant ligand. *Angew. Chem. Int. Ed.* **2022**, *134*, e202214108.
6 Sun, Y.; Ye, K.; Zhang, H.; Zhang, J.; Zhao, L.; Li, B.; Yang, G.; Yang, B.; Wang, Y.; Lai, S.-W.; Che, C.-M. Luminescent one-dimensional nanoscale materials with PtII···PtII interactions. *Angew. Chem. Int. Ed.* **2006**, *45*, 5610−5613.
7 Gambardella, P.; Dallmeyer, A.; Maiti, K.; Malagoli, M. C.; Eberhardt, W.; Kern, K.; Carbone, C. Ferromagnetism in one-dimensional monatomic metal chains. *Nature* **2002**, *416*, 301−304.
8 Wu, Y.; Zhang, Y.; Zeng, K.; Cheng, X.; Song, J.; Peng, H. A general strategy for the synthesis of metal-backboned molecules with different metals. *Angew. Chem. Int. Ed.* **2025**, *64*, e202502327.
9 Zhang, Y.; Zeng, K.; Wu, Y.; Huang, F.; Peng, H. Synthesis of nickel-backboned polymers by incorporating triazine groups. *Sci. Bull.* **2025**, *70*, 2223−2227.
10 Schmidbaur, H.; Schier, A. A briefing on aurophilicity. *Chem. Soc. Rev.* **2008**, *37*, 1931−1951.
11 Schmidbaur, H.; Schier, A. Aurophilic interactions as a subject of current research: an up-date. *Chem. Soc. Rev.* **2012**, *41*, 370−412.
12 Mao, H.-K.; Chen, X.-J.; Ding, Y.; Li, B.; Wang, L. Solids, liquids, and gases under high pressure. *Rev. Mod. Phys.* **2018**, *90*, 015007.
13 Guo, S.; Zhan, Y.; Lü, X. High-pressure research on optoelectronic materials: Insights from in situ characterization methods. *Matter Radiat. Extrem.* **2025**, *10*, 033802.
14 Bu, K.; Fu, T.; Wang, D.; Wang, R.; Guo, S.; Lü, X. Lone pair electron manipulation: a promising avenue for tuning properties in functional materials. *Eur. J. Inorg. Chem.* **2025**, *28*, e202400857.
15 Revol, G.; McCallum, T.; Morin, M.; Gagosz, F.; Barriault, L. Photoredox transformations with dimeric gold complexes. *Angew. Chem. Int. Ed.* **2013**, *52*, 13342−13345.
16 Tanase, T.; Chikanishi, M.; Morita, K.; Nakamae, K.; Kure, B.; Nakajima, T. Gold and silver chains supported by linear hexaphosphine ligands. *Chem–Asian J.* **2015**, *10*, 2619−2623.

17 He, B.; Cao, Y.; Lin, K.; Wang, Y.; Li, Z.; Yang, Y.; Zhao, Y.; Liu, X. Strong interactions between Au nanoparticles and $BiVO_4$ photoanode boosts hole extraction for photoelectrochemical water splitting. *Angew. Chem. Int. Ed.* **2024**, *136*, e202402435.
18 Liu, L.; Kuramochi, H.; Iwamura, M.; Nozaki, K.; Tahara, T. Localization of the Au–Au bond strength in the triplet excited state of the $[Au(CN)_2^-]$ oligomers revealed by ultrafast time-domain Raman spectroscopy. *Chem. Sci.* **2026**, *17*, 2676–2684.
19 Jin, M.; Chung, T. S.; Seki, T.; Ito, H.; Garcia-Garibay, M. A. Phosphorescence control mediated by molecular rotation and aurophilic interactions in amphidynamic crystals of 1,4-Bis[tri-(p-fluorophenyl)phosphane-gold(I)-ethynyl]benzene. *J. Am. Chem. Soc.* **2017**, *139*, 18115–18121.
20 Siddhant, K.; Rawat, A.; Matsumoto, K.; Nagai, Y.; Kobayashi, Y.; Prabusankar, G.; Tsutsumi, O. Aggregation-controlled dual-emissive room-temperature phosphorescence in gold(I) N-heterocyclic carbene complexes. *J. Phys. Chem. C* **2025**, *129*, 11131–11142.

https://doi.org/10.1007/s10118-026-3809-0